Electronic Supplementary information

Rigidity and Flexibility Dual-Network Polymer Electrolytes with Enhanced Interfacial Interaction to Accelerate Li+ Transfer

Qing Lv [1], Yuanyuan Sun [1], Sisi Jiang [1], Hao Ren [1], Yan Lin [2], Qi Li[1], Liping Lu [1], Mingbo Wu [1] and Zhongtao Li [1]*

[1] *State Key Laboratory of Heavy Oil Processing, College of Chemical Engineering, China University of Petroleum (East China) Qingdao 266580, P. R. China.*

[2] *Department of Chemistry, Tsinghua University, Beijing 100084, P. R. China*

Corresponding author: Zhongtao Li (liztao@upc.edu.cn)

Experimental Section

Preparation of SPE electrolyte. In a typical synthesis, 1.0 g Polyacrylonitrile (PAN, average Mw 149000~151000, Shanghai Aladdin Biochemical Technology Co., Ltd) was dissolved in 10 ml N, N-dimethylformamide (DMF) and then kept stirring for 12h at 50°C as the precursor solution for electrospinning. The working voltage, flow rate and collect distance during electrospinning is 13 kV, 15 μl/min and 20 cm, respectively. The membrane precursor was then put into an aqueous solution containing Bistrifluoromethanesulfonimidate (LiTFSI, 99%, Shanghai Macklin Biochemical Technology Co., Ltd), soaked overnight and dried, SPE electrolyte can be obtained. The casting film is prepared by dissolving PAN in NMP solvent, followed by casting the solution onto a polytetrafluoroethylene (PTFE) template, and then drying to obtain the film.

Preparation of PAN/CPTP electrolyte. 0.738 g piperazine (99%, Shanghai Macklin Biochemical Technology Co., Ltd) and 0.517 g cyanuric chloride (99%, Shanghai Aladdin Biochemical Technology Co., Ltd) were dissolved in 40 mL dioxane (99%, Shanghai Macklin Biochemical Technology Co., Ltd) and labelled as Solution A and Solution B. 2 mL Solution A was sprayed evenly on the SPE, then 2 mL of Solution B was sprayed evenly when the solvent was completely evaporated. The above operation was repeated until Solution A and Solution B were completely sprayed on the SPE to obtain the PAN/CPTP electrolyte membrane precursor. The PAN/CPTP electrolyte membrane precursor was washed with deionised water to remove excess HCl, put into

an aqueous solution containing LiTFSI, soaked overnight and dried. Then the electrolyte membrane was hot-pressed at 70 °C and 2000 kg for 5 h to further polymerise the CPTP to obtain the PAN/CPTP flexible composite electrolyte.

Material Characterizations. The crystal lattice of the synthesized electrolytes was characterized by X-ray diffractometer (XRD). Bruker D8 Advance X-ray diffractometer was used as the Cu Ka emission source (A = 1.5418a). Raman analysis was worked out by a Renishaw InVia Raman microscope with a 785 nm laser. The morphology and microstructure of the materials and the morphology of Li metal anodes of SPE and PAN/CPTP electrolytes after cycling was analyzed by the scanning electron microscopy (SEM, Hitachi S-4800 at 3 kV). The interaction between PAN and CPTP was studied by VERTEX 70 Fourier transform infrared (FT-IR) spectroscopy. ESCALAB 250 Xi X-ray photoelectron spectroscopy (XPS) was used to detect the surface of circulating lithium. Solid state nuclear magnetic resonance (NMR) (400 MHz) was used to characterize the coordination environment and interfacial exchange phenomena of lithium ions, the type of instrument used was Avance III. The specific surface area and pore size distribution of the CPTP were analyzed using Brunauer-Emmett-Teller (BET) analyzer. The type of BET instrument used was QuadraSorb SI.

Electrochemical measurements. The prepared SPE and PAN/CPTP membranes were cut into 19 mm diameter discs and placed in a glove box filled with argon atmosphere. In order to improve the poor solid-solid contact between the solid electrolyte and electrode 6 μl liquid electrolyte was added. The pristine ether-based electrolyte was

composed of 1 M LiTFSI in 1:1 (v/v) DME and DOL with 2 wt% LiNO$_3$ additive. To evaluate the electrochemical performance of electrolytes, 2030-type coin cells were assembled using lithium metal as anode and reference electrode. To prepare the positive electrode, 80 wt.% active materials, 10 wt.% super P, and 10 wt.% polyvinylidene fluoride (PVDF) were mixture with N-methyl-2-pyrrolidinone (NMP) solvent to gain a homogeneous slurry. Then, the slurry was casted on the aluminum foil and dried in vacuum at 60 °C for 12 h. The Al foil was then punched into 12 mm diameter disks and the active materials content was controlled around 2.5 mg cm^{-2}. The cells were assembled in an Ar filled glove box (Mikrouna, super 1220/750/900) with low levels of H$_2$O and O$_2$ (< 0.01 ppm). The cycle stability test was carried out on the Land CT2001A battery system. SS||SS cell was fabricated to test the ionic conductivity and the activation energy. Linear sweep voltammetry (LSV) is carried out by assembling Li||SS cells at a constant sweep rate of 1 mV s^{-1} to observe the variation of current with voltage (vs. Li/Li$^+$). Electrochemical impedance spectrum (EIS) was performed with a frequency range from 0.01 Hz to 100 kHz by using an electrochemical workstation. The symmetrical Li||Li cell for lithium plating/stripping test was cycled at a current density of 0.2 mA cm^{-2}.

Calculation Methods. Density functional theory (DFT) methods were used to carry out the Binding energy calculations through the Perdew-Burke-Ernzerhof (PBE) exchange-correlation functional in Vienna Ab Initio Simulation Package (VASP)[1–3]. The kinetic energy cutoff is set to be 500 eV for the plane-wave expansion after testing several cutoff energies. The convergence criterion for electronic structure iteration is

10^{-5} eV, and that for geometry optimization is 0.03 eV/Å. Considering the van der

Waals interactions between atoms, the Becke-Johnson method was applied for all

calculations[4]. The interface was built by matching the COF supercell with amorphous

PAN cluster and TFSI anion, to avoid interactions between the slab, a vacuum thickness

of 20 Å was added upon the surface.

E(TFSI$^-$ on PAN/CPTP) = E(TFSI$^-$/PAN/CPTP) - E(TFSI$^-$) - E(PAN/CPTP)

where E(TFSI$^-$/PAN/CPTP) is the totoal energy of the optimized PAN/CPTP adsorbed

with TFSI$^-$, while E(TFSI$^-$)and E(PAN/CPTP) are the optimized TFSI$^-$ and PAN/CPTP

complex surface, respectively. The calculation adsorption energy of TFSI$^-$ to the PAN

is the same as the above procedure.

The finite element simulation of the battery cell was carried out by applying

COMSOL. The transient study of lithium symmetric batteries using the lithium-ion

battery physical field interface in order to represent the variation of its electrolyte salt

concentration, showing the hypothetical equations as follows:

$$\frac{\partial c_1}{\partial t} + \nabla \cdot N_1 = R_1$$

$$\dots \dots$$

$$\nabla \cdot i_1 = Q_1$$

$$\dots \dots$$

$$i_1 = -\sigma_1 \nabla \varphi_1 + \frac{2\sigma_1 RT}{F}(1 + \frac{\partial lnf}{\partial lnc_1})(1 - t_+)\nabla lnc_1$$

$$N_1 = -D_1 \nabla c_1 + \frac{i_1 t_+}{F}$$

The temperature was taken as room temperature i.e. 298.15 K. The global coordinate system was chosen and the conductivity of the electrolyte used σ_1 and the lithium ion mobility number t_+ were the same as previously described. A voltage of 10 mV was applied on one side for 30 s in 0.1 s steps and the other side was allowed to ground. The electrolyte thickness was set to 50 μm, the lithium metal thickness was set to 10 μm on both sides, and the initial salt concentration was set to 500 mol m^{-3}

Supplementary figures
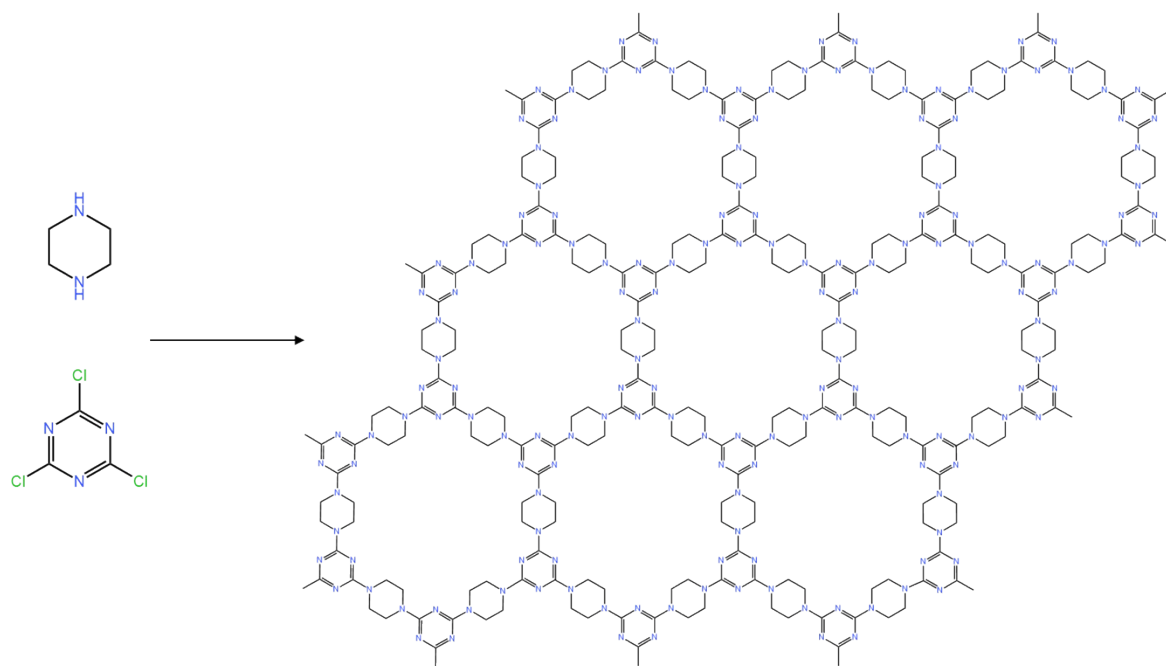
Fig. S1 Polymerisation of CPTP occurring on PAN spinning surface.
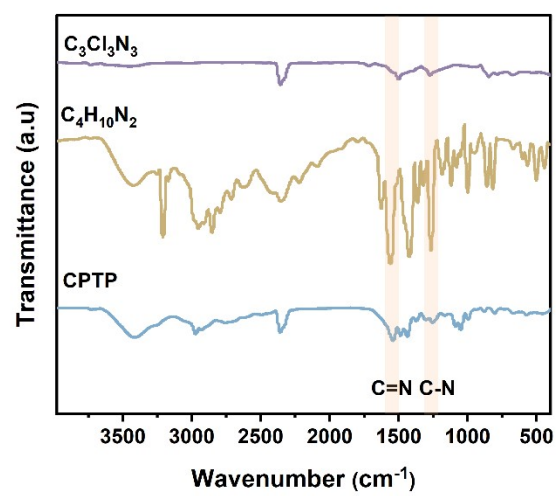
Fig. S2 FTIR of CPTP.
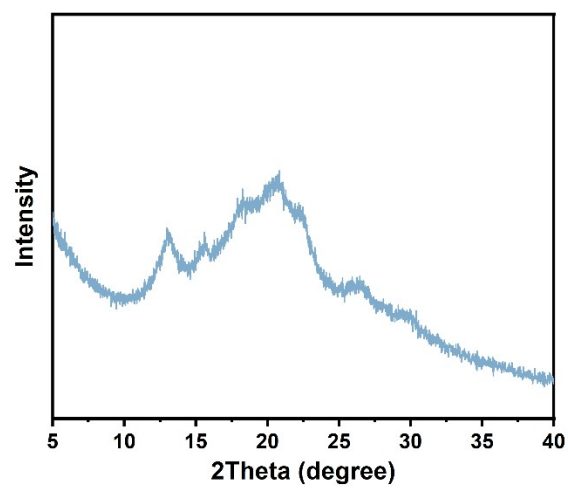
Fig. S3 XRD of CPTP.
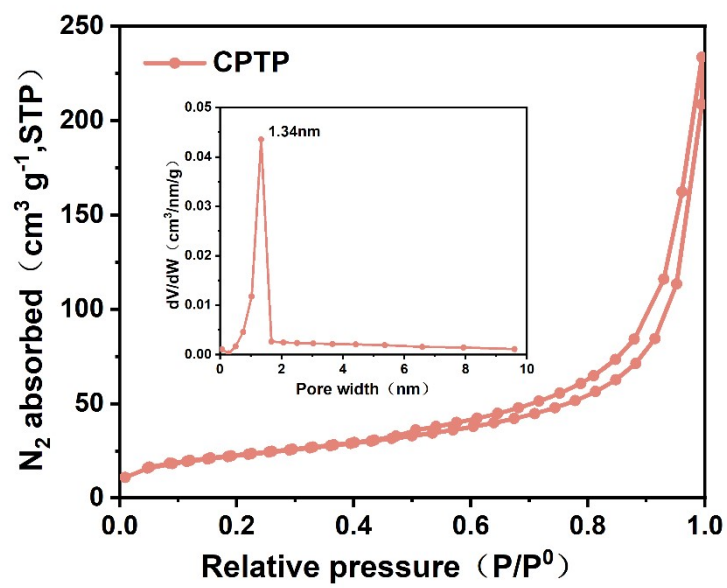
Fig. S4 Nitrogen adsorption-desorption isotherm curves of CPTP.
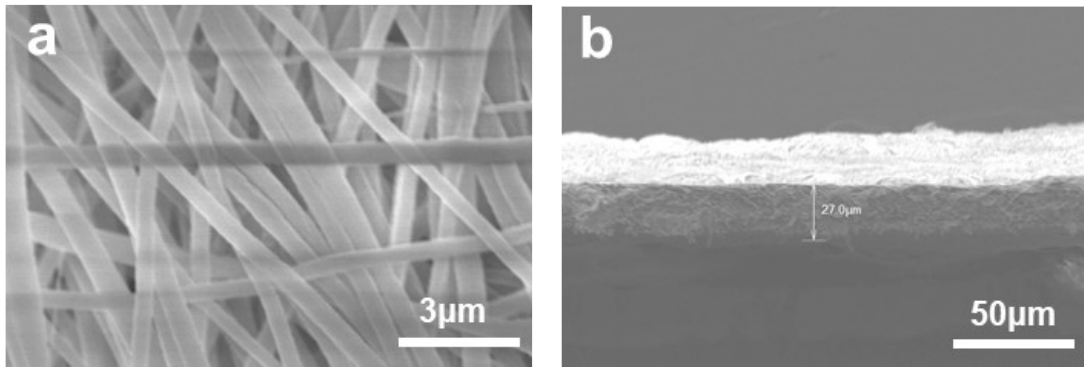
Fig. S5 Surface(a) and cross-section(b) SEM images of SPE.
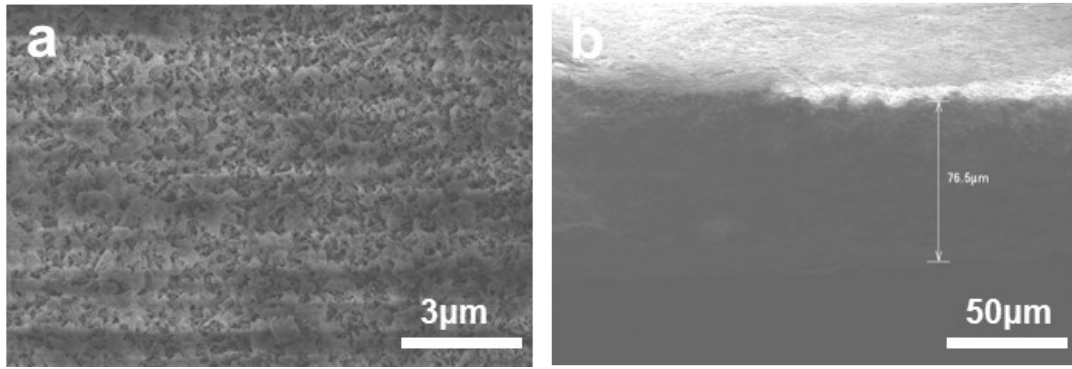
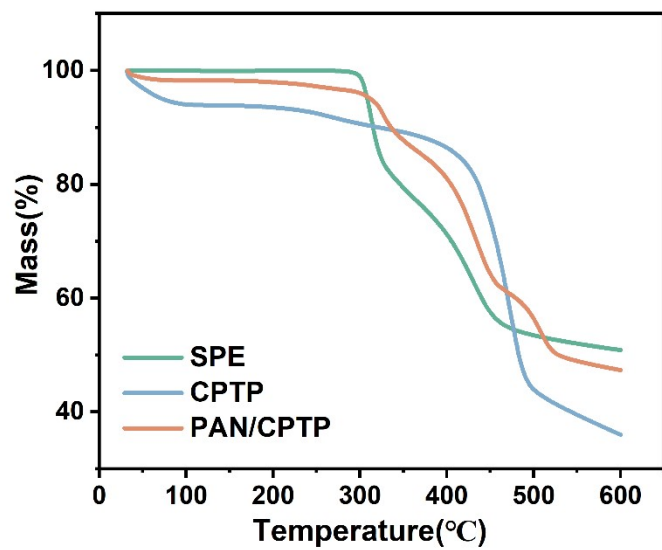**Fig. S6** Surface(a) and cross-section(b) SEM images of PAN/CPTP.

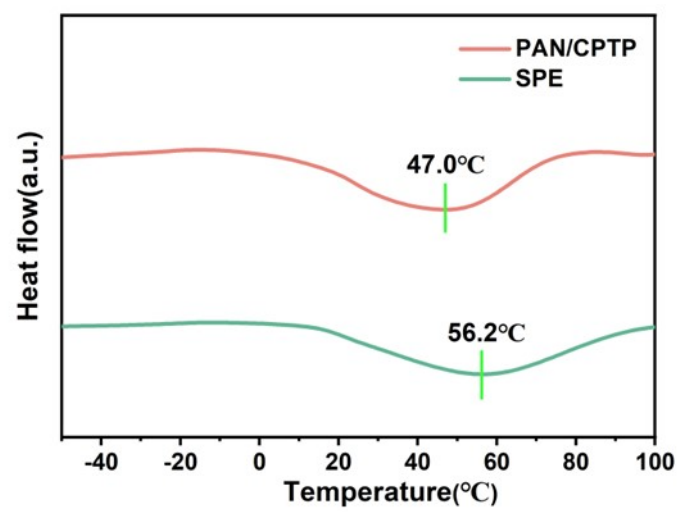**Fig. S7** Thermal gravimetric analysis of PAN, CPTP and PAN/CPTP.
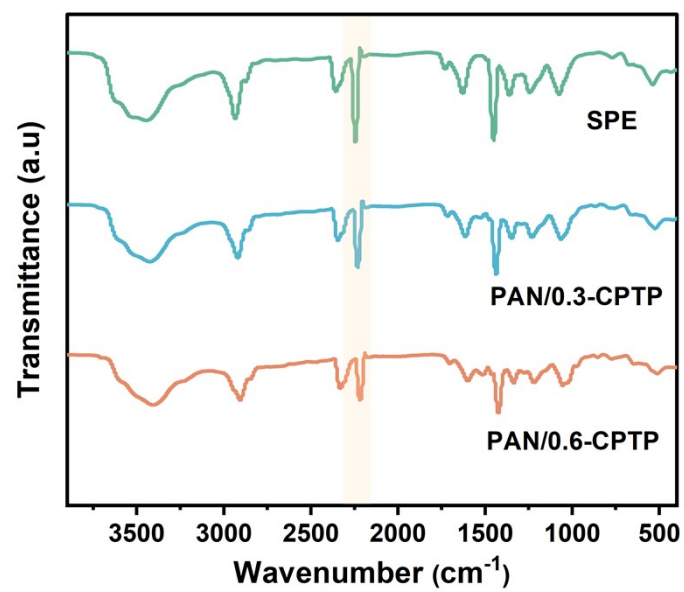
Fig. S8 DSC curves of SPE and PAN/CPTP.
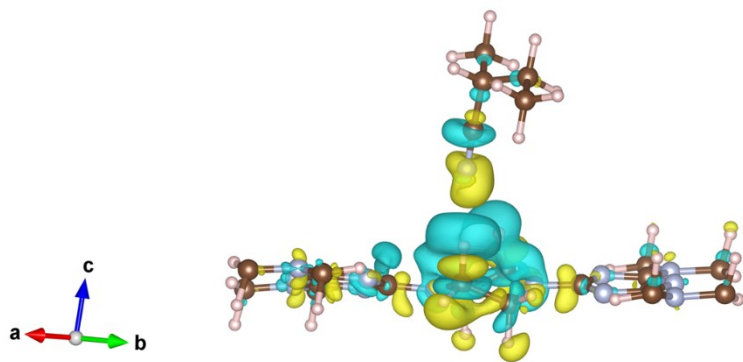
Fig.S9 FTIR of different contents of CPTP.

Fig.S10 Differential charge diagrams for PAN and CPTP
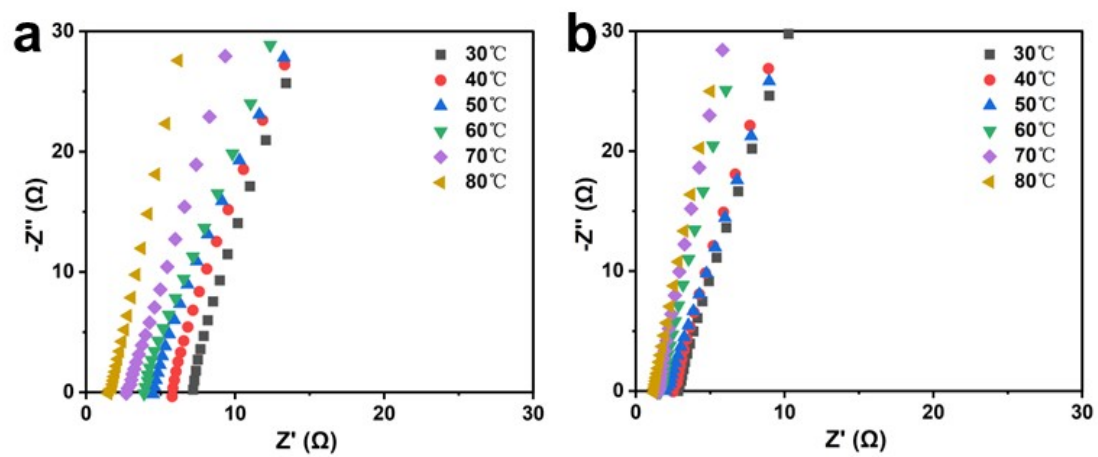
Fig. S11 Impedance plots of SPE (a) and PAN/CPTP (b) at different temperatures.
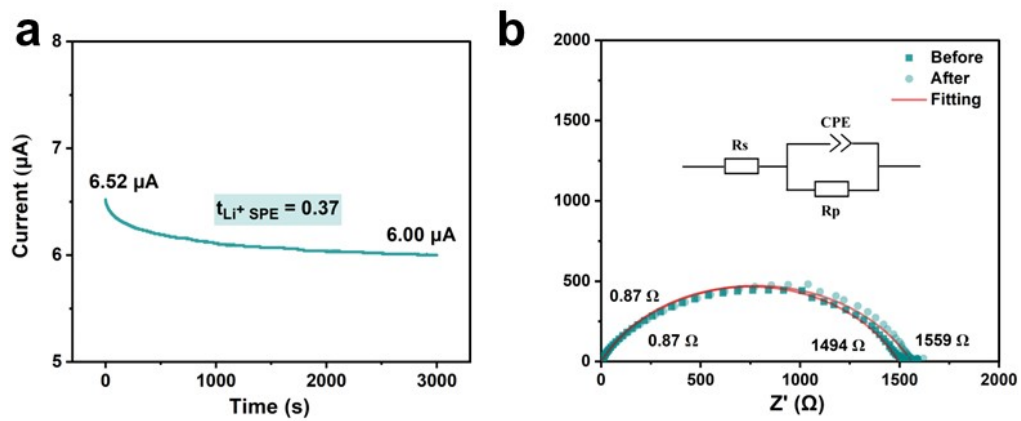
Fig. S12 Polarization curve (a) and impedance diagram of the battery before and after polarization for Li//SPE//Li (b).
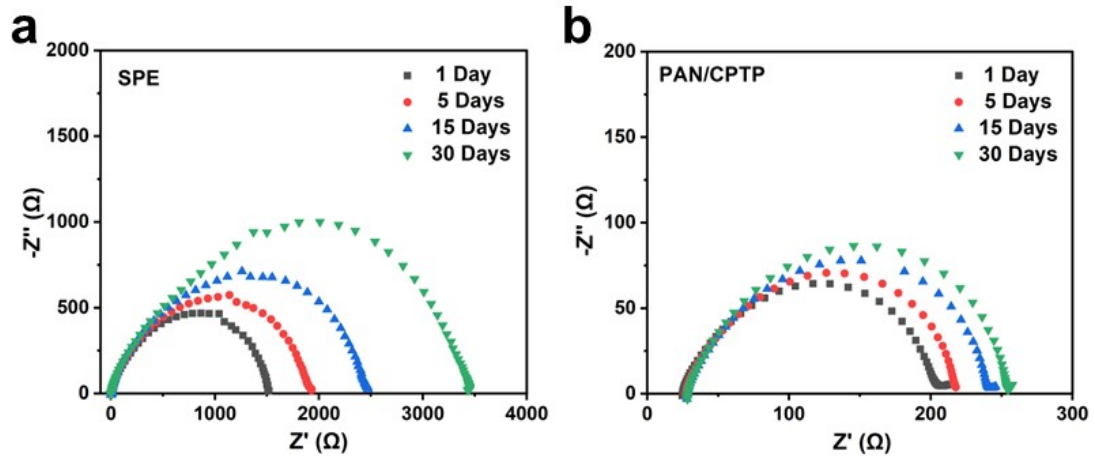
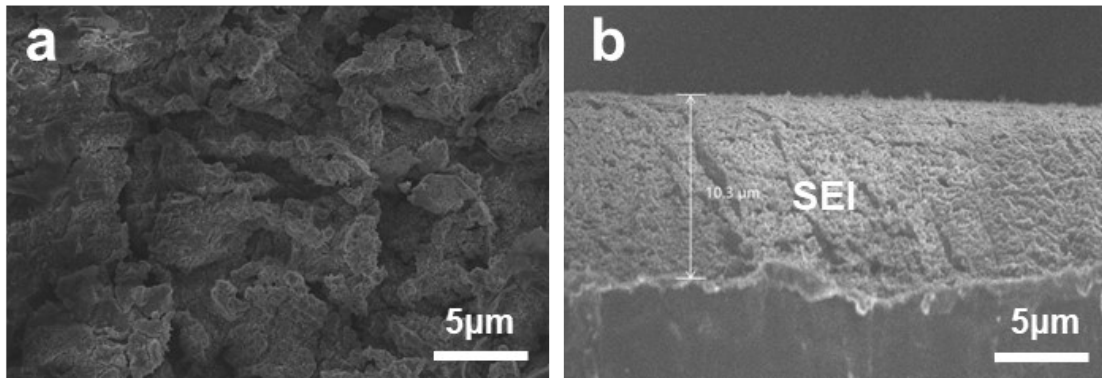**Fig. S13** Impedance versus time plots for SPE (a) and PAN/CPTP (b).

Fig. S14 SEM images of lithium metal surface (a) and cross-section (b) of Li//SPE//Li cells after 50 cycles.
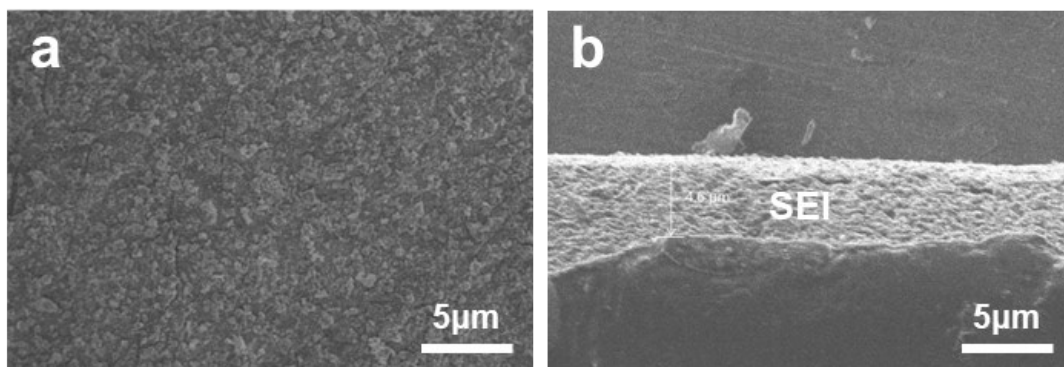
Fig. S15 SEM images of lithium metal surface (a) and cross-section (b) of Li//PAN/CPTP//Li cells after 50 cycles.
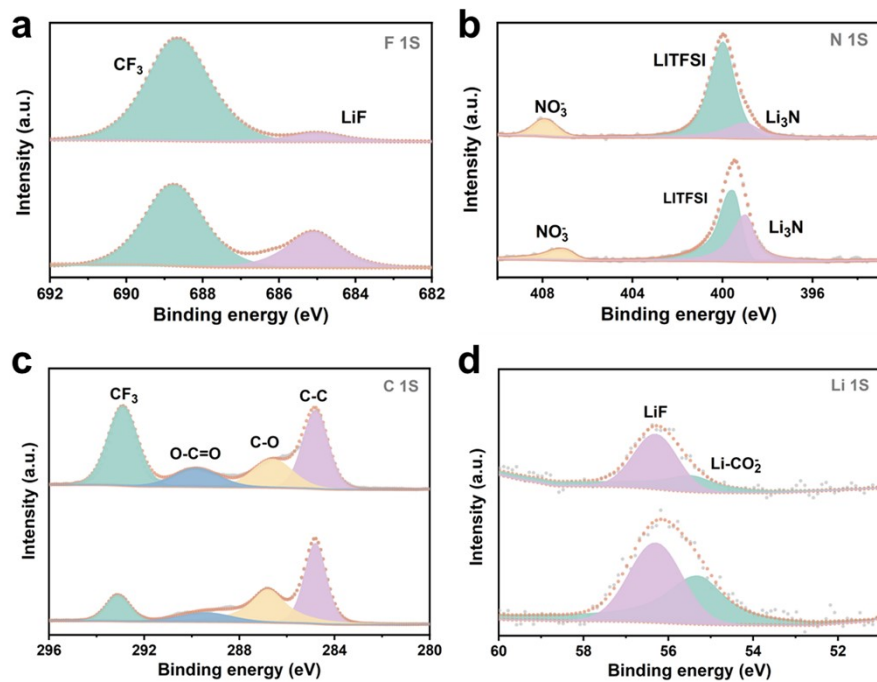
Fig. S16 XPS analysis of lithium metal surfaces of Li//SPE//Li (top) and Li//PAN/CPTP// Li (bottom) cells after 50 cycles. (a) F 1s; (b) N 1s; (c) C 1s; (d) Li 1s.

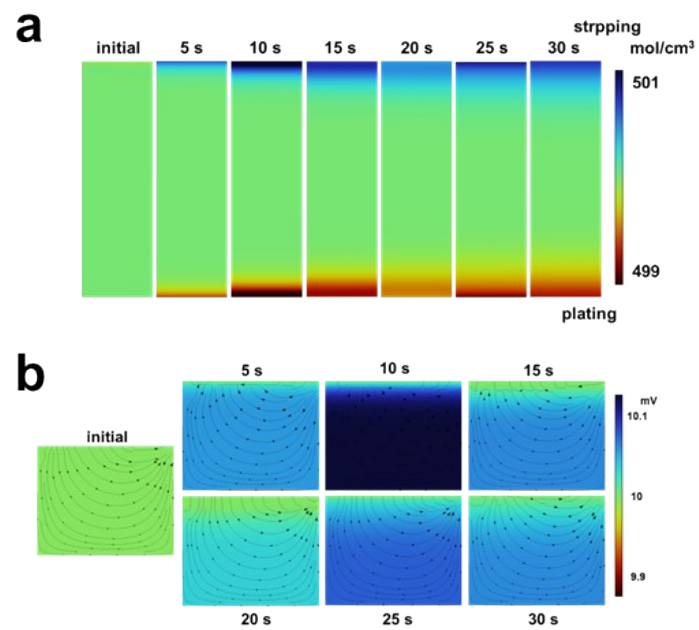**Fig. S17** COMSOL simulation of electrolyte concentration distribution (a) and potential and current vector distributions (b) for Li//SPE//Li cells.
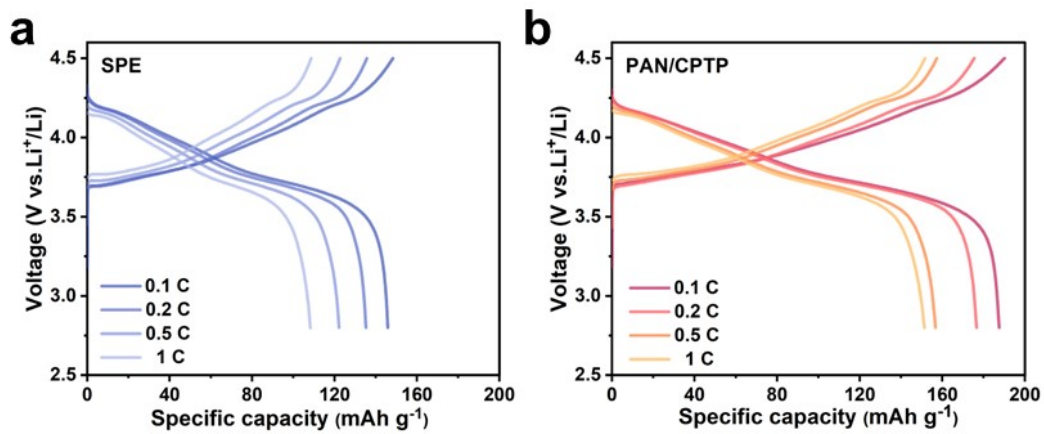
Fig. S18 Charge-discharge curves of NCM811//SPE//Li (a) and NCM811//PAN/CPTP//Li (b) cells at different rates.
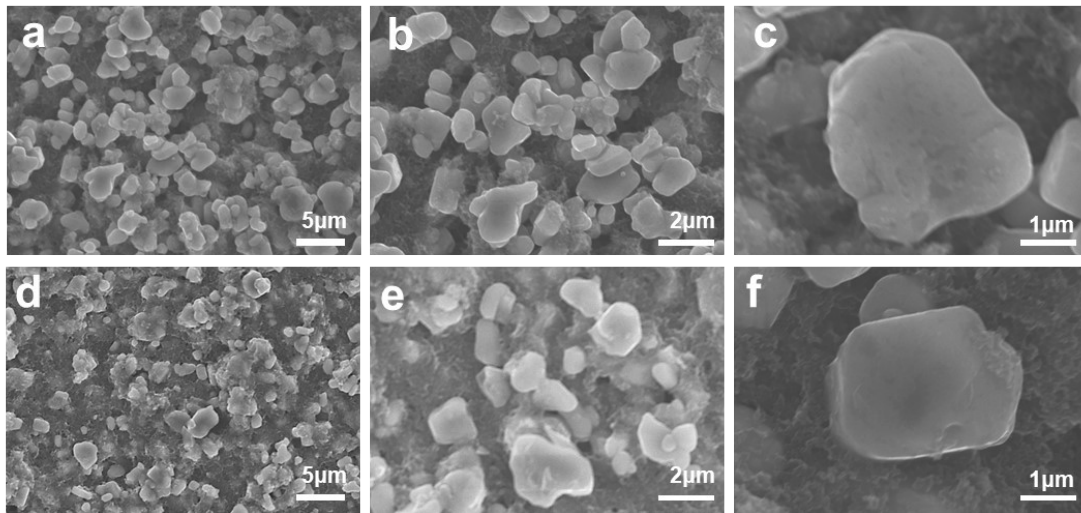
Fig. S19 SEM images of NCM811 electrode sheets of NCM811//PAN/CPTP//Li cells before (a-c) and after 50 cycles (d-f) at 1C.
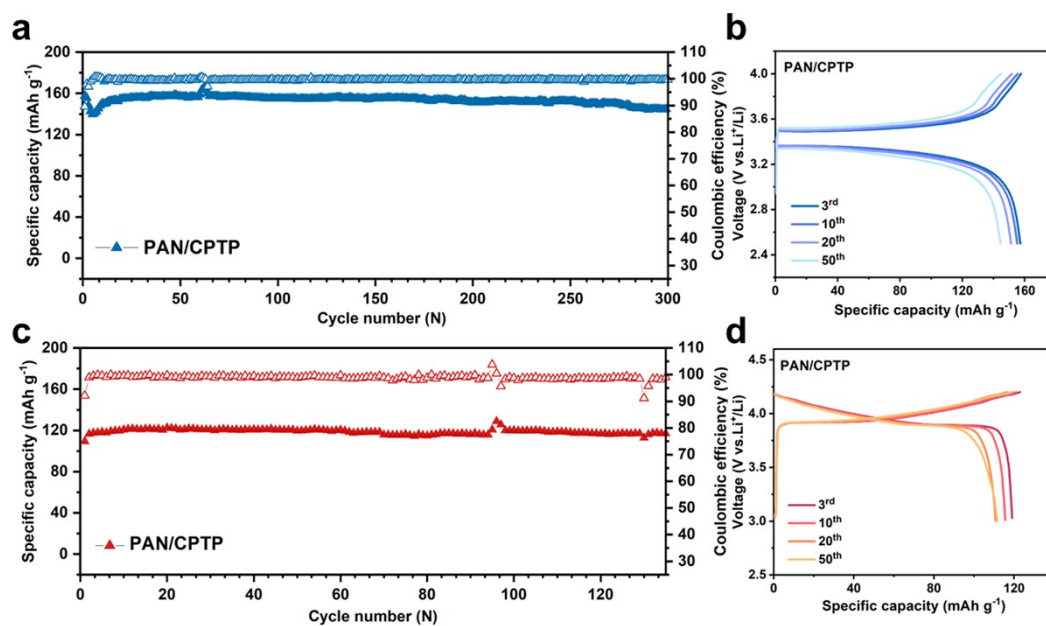
Fig. S20 Cycling performance (a) and charge/discharge voltage distribution (b) of LiFePO$_4$//PAN/CPTP//Li cells at 0.5C, 2.5-4V; Cycling performance (c) and charge/discharge voltage distribution (d) of LiCoO$_2$//PAN/CPTP//Li cells at 0.5C, 3-4.3V.

Fig. S21 Performance diagram of silicon carbon soft pack battery assembled by PAN/CPTP.

Supplementary tables

Table S1 Crystallinity analysis of SPE and PAN/CPTP

Electrolytes	T_m (°C)	$\triangle H_m$ (J g^{-1})	χ_c (%)
SPE	56.2	59.49	29.75
PAN/CPTP	47.0	58.25	14.56

Table S2 The comparison key properties and cycling performance for polymer electrolyte

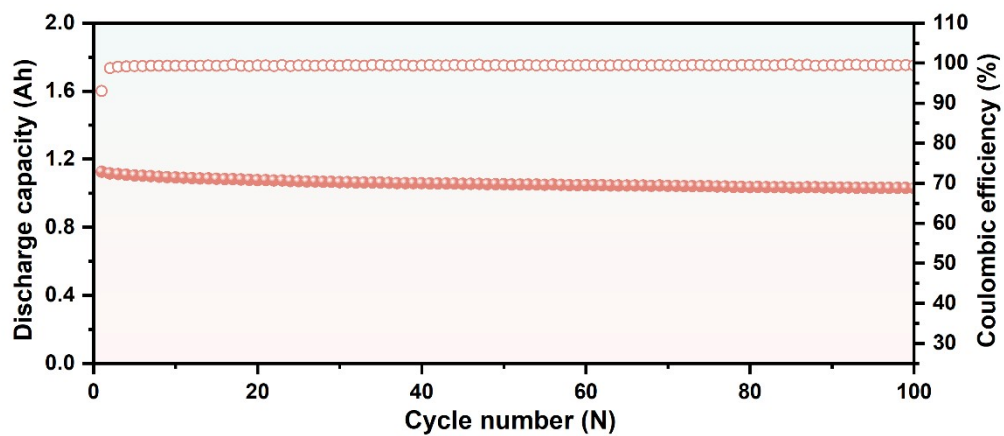| Electrolytes	Conductivity (mS cm^{-1})	t_{Li+}	Anode/Cathode	Rate(C)	Cutoff voltage(V)	Cycle	Capacity retention (%)	Ref.
PAN@ZIF/IL	1.3@30°C	0.82	Li/NCM811	2	4.3	100@RT	88	[5]
FPCSPE3-40	0.05@25°C	0.44	Li/NCM811	0.1	4.5	200/300@25°C	85/70	[6]
PEGDME-4	0.15@60°C	N/A	Li/NCM523	0.2	4.5	200@N/A	59	[7]
PT-PEO-PT	0.11@40°C	0.54	Li/NCM523	0.2	4.2	75@40°C	80	[8]
FMC-ASPE-Li	0.64@80°C	0.88	Li/NCM811	0.3	4.2	100@70°C	87	[9]
SS-PPCE/PAN-3%	1.7@30°C	0.51	Li/NCM811	0.1	4.3	50@RT	72.2	[10]
C-SPE	0.13@25°C	0.62	Li/LCO	1	4.5	200@RT	83.9	[11]
IPLL-SSE	2.06@25°C	0.5	Li/NCM523	0.05	4.5	30@25°C	89.2	[12]
PAN-LLZTO-PEO	0.26@30°C	0.6	Li/NCM111	0.2	4.2	100@30°C	65	[13]
PI-LLZTO/PVDF	0.12@25°C	0.51	Li/NCM523	0.1	4.3	80@25°C	94.9	[14]
PAN/CPTP	**0.94@30°C**	**0.89**	**Li/NCM811**	**0.5**	**4.5**	**200@30°C**	**85**	**This work**
PAN/CPTP	**0.94@30°C**	**0.89**	**Li/NCM811**	**1**	**4.5**	**100@30°C**	**86.9**	**This work**

References

1 G. Kresse and J. Furthmüller, *Phys. Rev. B*, 1996, **54**, 11169–11186.

2 G. Kresse and D. Joubert, *Phys. Rev. B*, 1999, **59**, 1758–1775.

3 J. P. Perdew, K. Burke and M. Ernzerhof, *Phys. Rev. Lett.*, 1996, **77**, 3865–3868.

4 A. Tkatchenko and M. Scheffler, *Phys. Rev. Lett.*, 2009, **102**, 073005.

5 X. Zhang, Q. Su, G. Du, B. Xu, S. Wang, Z. Chen, L. Wang, W. Huang and H. Pang, *Angew. Chem. Int. Ed.*, 2023, **62**, e202304947.

6 Y. Wang, S. Chen, Z. Li, C. Peng, Y. Li and W. Feng, *Energy Storage Mater.*, 2022, **45**, 474–483.

7 X. Yang, M. Jiang, X. Gao, D. Bao, Q. Sun, N. Holmes, H. Duan, S. Mukherjee, K. Adair, C. Zhao, J. Liang, W. Li, J. Li, Y. Liu, H. Huang, L. Zhang, S. Lu, Q. Lu, R. Li, C. V. Singh and X. Sun, *Energy Environ. Sci.*, 2020, **13**, 1318–1325.

8 J. Zheng, C. Sun, Z. Wang, S. Liu, B. An, Z. Sun and F. Li, *Angew. Chem. Int. Ed.*, 2021, **60**, 18448–18453.

9 Y. Su, X. Rong, A. Gao, Y. Liu, J. Li, M. Mao, X. Qi, G. Chai, Q. Zhang, L. Suo, L. Gu, H. Li, X. Huang, L. Chen, B. Liu and Y.-S. Hu, *Nat. Commun.*, 2022, **13**, 4181.

10 Q. Liu, Y. Dan, M. Kong, Y. Niu and G. Li, *Small*, 2023, **19**, 2300118.

11 J. Liu, Y. Zhang, H. Ji, J. Zhang, P. Zhou, Y. Cao, J. Zhou, C. Yan and T. Qian, *Adv. Sci.*, 2022, **9**, 2200390.

12 Z. Ren, J. Li, Y. Gong, C. Shi, J. Liang, Y. Li, C. He, Q. Zhang and X. Ren, *Energy Storage Mater.*, 2022, **51**, 130–138.

13 L. Gao, B. Tang, H. Jiang, Z. Xie, J. Wei and Z. Zhou, *Adv. Sustainable Syst.*, 2022, **6**, 2100389.

14 J. Hu, P. He, B. Zhang, B. Wang and L.-Z. Fan, *Energy Storage Mater.*, 2020, **26**, 283–289.